

Flow in bedrock canyons

Jeremy G. Venditti¹, Colin D. Rennie², James Bomhof², Ryan W. Bradley¹, Malcolm Little¹ & Michael Church³

Bedrock erosion in rivers sets the pace of landscape evolution, influences the evolution of orogens and determines the size, shape and relief of mountains^{1,2}. A variety of models link fluid flow and sediment transport processes to bedrock incision in canyons. The model components that represent sediment transport processes are increasingly well developed^{3–5}. In contrast, the model components being used to represent fluid flow are largely untested because there are no observations of the flow structure in bedrock canyons. Here we present a 524-kilometre, continuous centreline, acoustic Doppler current profiler survey of the Fraser Canyon in western Canada, which includes 42 individual bedrock canyons. Our observations of three-dimensional flow structure reveal that, as water enters the canyons, a high-velocity core follows the bed surface, causing a velocity inversion (high velocities near the bed and low velocities at the surface). The plunging water then upwells along the canyon walls, resulting in counter-rotating, along-stream coherent flow structures that diverge near the bed. The resulting flow structure promotes deep scour in the bedrock channel floor and undercutting of the canyon walls. This provides a mechanism for channel widening and ensures that the base of the walls is swept clear of the debris that is often deposited there, keeping the walls nearly vertical. These observations reveal that the flow structure in bedrock canyons is more complex than assumed in the models presently used. Fluid flow models that capture the essence of the three-dimensional flow field, using simple phenomenological rules that are computationally tractable, are required to capture the dynamic coupling between flow, bedrock erosion and solid-Earth dynamics.

The linkages between the uplift of mountains, tectonics and climate are critical for understanding how surface processes affect solid-Earth dynamics and remain one of the primary open questions in Earth science. To understand these linkages we must examine the large-scale drivers of bedrock incision by rivers^{2,6–8}. Large-scale bedrock canyons in actively uplifting terrain link tectonics, climate and topography. Bedrock incision in canyons at the local scale happens through a combination of plucking (removal of blocks of rock from the river bed or banks) and various types of abrasion by sediment particles. Although there is some uncertainty about their relative importance², there are models for abrasion by bedload³, suspended load⁴ and plucking⁵. The flow parameterization most often used in bedrock erosion models is based on stream power^{6,8–12}. Although this approach allows for computationally tractable landscape-scale modelling over long periods and at large scales^{6,8}, flow and sediment transport dynamics are not considered, making the approach of limited value for the prediction of bedrock channel morphology and dynamics. Moreover, the stream power approach masks the fluid processes that drive the sediment movements that cause bedrock erosion. Mechanistic parameterizations of the flow use simplifying assumptions of steady, uniform flow^{13–16} and empirical frictional relations^{17,18}, because full representations of coupled fluid and sediment dynamics are not currently computationally tractable at large scale. More advanced models of boundary shear stress in channel cross-sections have recently been incorporated into bedrock river models that allow modelling of channel shape^{16,19,20}. However, none of these flow models has been tested because there are no field observations of the flow structure in bedrock canyons. Access to these rivers is difficult and

the instrumentation necessary for observations has only relatively recently been adapted from oceanographic research for use in rivers.

To address this gap in our understanding of bedrock rivers, we undertook a 524-km-long continuous centerline acoustic Doppler current profiler (ADCP) survey of the Fraser Canyon, British Columbia, Canada (see Methods). An ADCP provides profiles of three-dimensional velocity measured in Earth coordinates (Easting, Northing, vertical) and bed elevation at discrete intervals. From this we calculate the downstream horizontal velocity magnitude ($U_e^2 + U_n^2$)^{0.5} (where U_e and U_n are the Easting and Northing velocities) and the vertical velocity, which is orthogonal to the horizontal plane. The Fraser Canyon is a geographical region along the Fraser River characterized by a series of 42 individual canyons where the river crosses the Interior Plateau of British Columbia and flows along a fault between the Coast and Cascade mountain ranges (Extended Data Fig. 1). The channel alternates between alluvial and bedrock-bound reaches, the latter of which comprise about 18% of the river length. About 10% of the total length is ‘canyons’—that is, rock-bound, conspicuously narrow reaches. The along-stream profiles of the canyons all show a drop in bed elevation, forming a deeply scoured pool as the channel is constricted (Fig. 1a), with deeper pools formed where the channel constriction is greater. The channel width to mean depth ratios (w/h) of the canyons vary between 2.3 and 17.3 (mean of 6.9; ratios of >20 are common for alluvial channels²¹; in unconfined reaches of Fraser River the average is 52). Canyon width to maximum depth ratios (w/h_{\max}) varied from 1.5 to 10.1 during our surveys (at higher flows, these values will decline because the channel is laterally constricted).

As flow is confined in a canyon, the cross-sectional area decreases and mass-balance dictates that the flow must accelerate. But if canyon floor elevation declines rapidly downstream, increasing the depth, the flow will decelerate. The deceleration should be more pronounced in narrow bedrock canyons where additional drag from the walls may be of the same magnitude as the drag exerted from the channel bed¹⁶. In the widest canyons of the Fraser, flow decelerates uniformly with depth as flow enters the canyons and accelerates as flow exits the canyons. In the narrower canyons, a high-velocity core appears to plunge below the water surface and follow the bed topography down into the pool (Fig. 1a). The high-velocity core dissipates with distance downstream, but with each narrowing of the canyons, the plunging velocity core reappears. The pattern of multiple plunging high-velocity cores observed in Iron Canyon (Fig. 1a) is typical of the narrow bedrock canyons of the Fraser River.

What could cause a plunging high-velocity core? The structure of flow along the centreline is a manifestation of the three-dimensional flow field. Cross-sections through three-dimensional grids of measured spatially distributed velocity fields in the canyons (Fig. 2 and Supplementary Videos 1 and 2; see Methods for details of data processing) show there is a clear velocity inversion (low-velocity fluid at the top of the water column and high-velocity fluid at the bottom; Fig. 1b) that corresponds to negative vertical velocities along the channel centreline. To compensate for this downward flow, upwelling along the canyon walls brings highly turbulent, low-velocity fluid up from near the bed, causing the inversion. Our observations suggest that these upwellings take the form of large and powerful, intermittent coherent flow structures that form boils at the water surface²². These structures represent deviations

¹Department of Geography, Simon Fraser University, Burnaby, British Columbia V5A 1S6, Canada. ²Department of Civil Engineering, University of Ottawa, Ottawa, Ontario K1N 6N5, Canada. ³Department of Geography, The University of British Columbia, Vancouver, British Columbia V6T 1Z2, Canada.

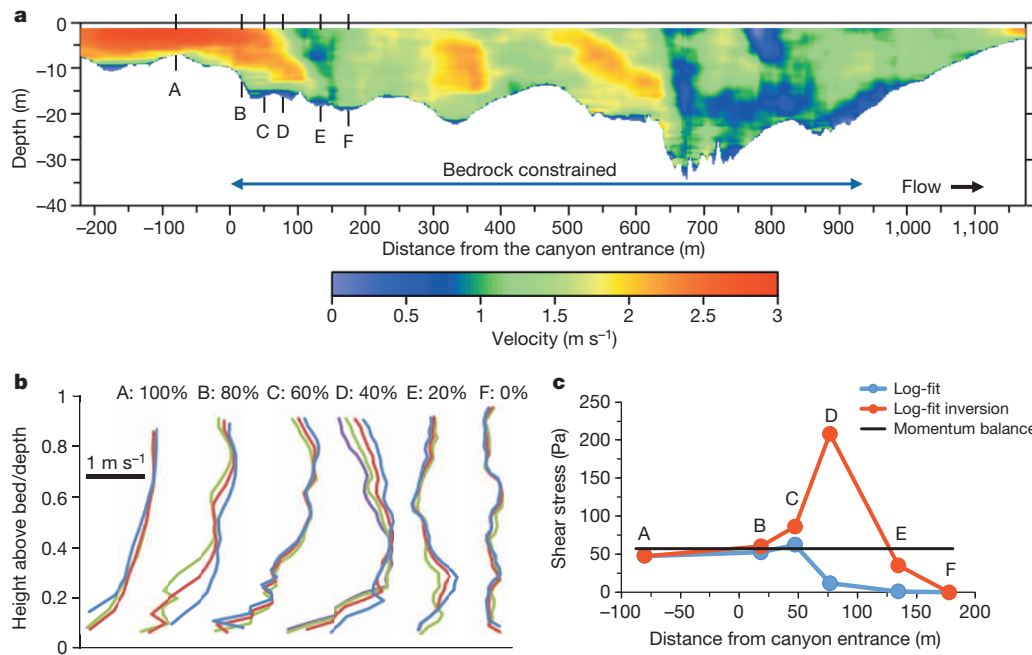


Figure 1 | Centreline transects of flow through a narrow bedrock canyon of the Fraser River. **a**, Primary downstream velocity (colour scale) in Iron Canyon ($w/h = 4.2$, $w/h_{\max} = 1.7$), the second narrowest of the Fraser canyons. Primary downstream velocity is the horizontal velocity magnitude calculated from Easting and Northing velocity components, rotated to minimize the depth-averaged, cross-channel velocity of each profile. **b**, Velocity profiles

along the entrance to the canyon at locations corresponding to the letters A to F in **a**. The approximate height of the velocity inversion is given as a percentage of flow depth. **c**, Shear stresses calculated from reach-averaged momentum balance, velocity profiles through the whole water column (log-fit) and the lower linear portion of the velocity profile below the inversion (log-fit inversion).

from the mean flow, and are advected towards the channel centre, dissipating into the mean flow as the channel expands downstream.

We hypothesize that the observed flow structure is caused by convective deceleration as flow exits the channel constriction and enters the scour hole. Experiments on flow into pools²³ with a morphology similar to our bedrock canyons revealed downward-directed mean velocity as flow expanded into the pool. Furthermore, the same pattern of secondary circulation was observed. This included lateral convergence at the water surface during deceleration in the pool. In pool experiments, downwelling in the centre of the channel and upwelling along the channel walls also occurred, which has been demonstrated to take the form of

intermittent coherent flow structures in similar experiments²⁴. This pattern of secondary flow is typical in narrow channels²⁵ and has been attributed to anisotropy of turbulence at channel boundaries and the free surface. We suspect that a similar process occurs in the bedrock canyons of the Fraser River, whereby upwelling along the channel walls and flow convergence at the surface leads to relatively low-speed, highly turbulent fluid at the water surface in the channel centre downstream of the constriction. The upwelling reduces near-bed dynamic pressure²⁶, which will encourage the higher-speed flow entering the canyons to advect along the floor, and a positive feedback whereby the high-speed fluid near the bed contributes to intense upwelling along the walls. The initiation of this flow structure in a bedrock channel is probably caused by the lateral constriction, forcing a canyon to deepen until it reaches morphodynamic equilibrium with the near-bed flow (and the sediment transport responsible for incision).

We expect the three-dimensional flow processes observed in the canyons of the Fraser River to be applicable to many canyon-bound rivers worldwide. This is because significant changes in channel width, which we argue here drive convective deceleration and flow inversion, are common. This suggests a model of flow in narrow bedrock canyons (Fig. 3) that is very different from what is currently accepted. Velocity inversions and the associated plunging high-velocity cores (Fig. 3a) cause steeper near-bed velocity gradients than would occur if the flow decelerated uniformly into canyons. This would tend to increase vertical incision and formation of scour holes because shear stress, which drives the sediment transport processes responsible for incision, scales as $\tau \propto (du/dz)^2$ (where u is the velocity at height z above the bed).

For example, reach-averaged shear stress in Iron Canyon, calculated from the one-dimensional momentum balance for steady, uniform flow (see Methods), was 115 Pa, roughly half of which is applied to the walls because it is narrow relative to its depth¹⁶. Velocity profiles through the whole water column predict shear stress to increase slightly and then decline moving into Iron Canyon (Fig. 1c), but this also requires steady, uniform flow. On the other hand, using the linear portion of near-bed velocity gradients, below the inversion inflection point, produces the most

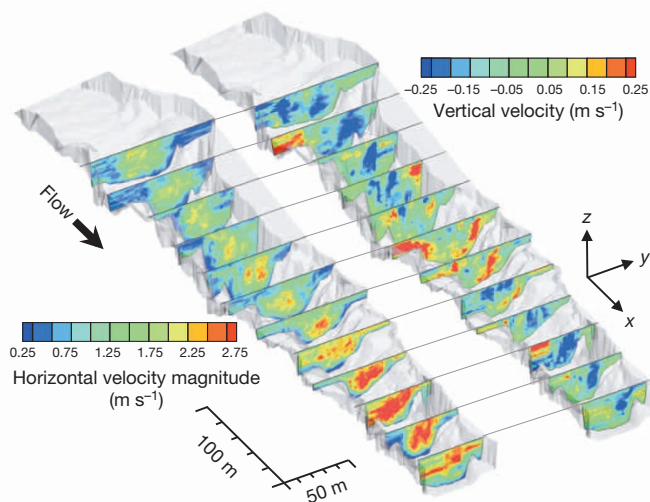


Figure 2 | Cross-sections of horizontal velocity magnitude and vertical velocity in Black Canyon downstream of a constriction. See Supplementary Video 1 of the horizontal velocity magnitude and Supplementary Video 2 of vertical velocity fields through the whole measurement section.

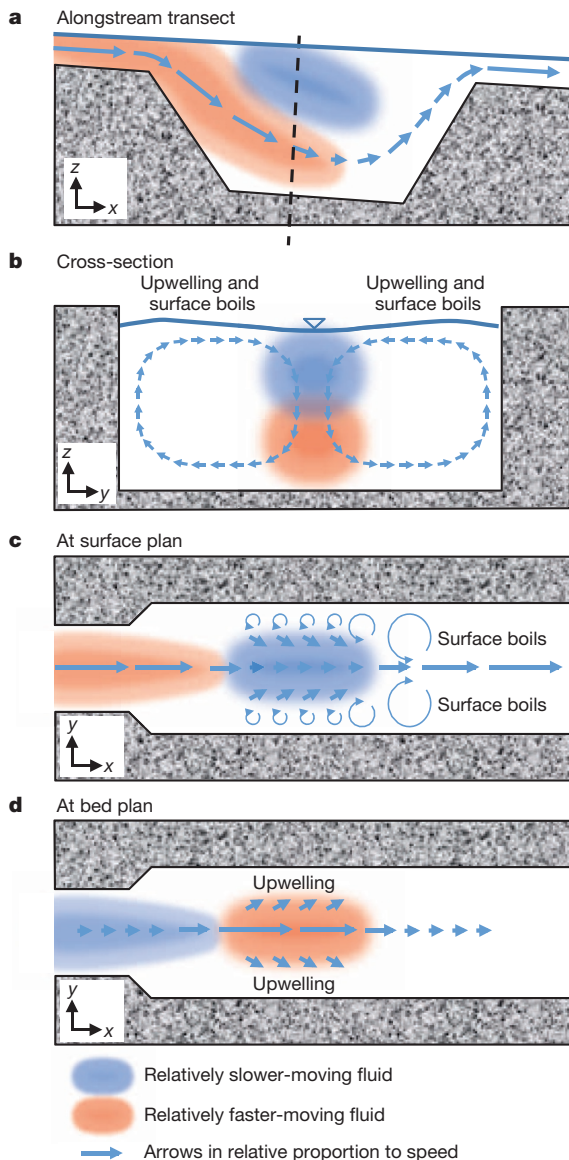


Figure 3 | Conceptual model of flow in a bedrock canyon. **a**, Alongstream section through the flow field showing the apparent plunging velocity core. **b**, Cross-section at dashed line in panel **a** showing velocity inversion and the observed water surface profile caused by flow paths. **c**, Flow pattern at the water surface showing accelerated, then convergent decelerated flow in the alongstream direction and intermittent surface boils produced by large-scale coherent flow structures. **d**, Flow pattern at the bed showing decelerated, then divergent accelerated flow and zones of upwelling, which take the form of large-scale coherent flow structures. x , y and z are the streamwise, cross-stream and vertical velocity directions, respectively. The diagrams are vertically and horizontally exaggerated.

accurate representations of local shear stress (see Methods). This approximation indicates that shear stress was 47 Pa at the canyon entrance, rose to 208 Pa along the entrance slope, and then declined to nearly zero in the bottom of the scour hole where the flow changes from convectively decelerating to accelerating (Fig. 1c).

The larger shear stress along the entrance slope to a canyon would tend to focus erosion there, resulting in an upstream migrating scour hole that resembles a submerged knickpoint. Where the plunging high-velocity core extends beyond the entrance slope, a canyon will deepen until it reaches morphodynamic equilibrium. The counter-rotating secondary flow structure (Fig. 3b) causes decelerated surface flow along a channel centreline (Fig. 3c). The vertical upwelling along canyon walls (Fig. 3b) and divergent flow at the bed (Fig. 3d) can cause centreline ridges along

a canyon floor, which we observed in some of the Fraser canyons. Divergent flow at the bed also provides a mechanism for undercutting canyon walls (as has been observed experimentally^{27,28}). Failure of undercut rock could promote channel widening over long timescales if upstream knickpoint migration occurred over a lesser time frame. The general pattern of fluid motion would also tend to keep the base of canyon walls swept clean of wasted debris, maintaining near-vertical walls.

The observed patterns of flow in the Fraser canyons suggest that modelling canyon morphodynamics and evolution requires more detailed understanding of the flow dynamics that drive sediment transport in canyons. The steep near-bed velocity gradients along plunging velocity cores cause correspondingly higher and lower local shear stresses than would be predicted from reach-averaged shear stress for steady uniform flow, calculated using mean velocity and a flow resistance equation, or log-normal velocity profiles that extend from the bed to the water surface. These locally higher and lower shear stresses may average out over the length of canyons, but the morphology of a canyon and patterns of incision are driven by the spatial variations in the shear stress. Erosion rates tend to scale with bed shear stress to a power greater than unity^{3–5}, so even if local bed shear stresses average out over the length of a canyon, local erosion rates will not average out, leading to larger canyon erosion rates even when averaged over long timescales. Further observations, along with hydrodynamic modelling that captures both the secondary circulation and the dynamics of the upwelling coherent flow structures, are required to determine how best to abstract these insights on the complexity of flow in bedrock canyons over the temporal and spatial scales of drainage basin organization⁸ and orogen development¹.

Online Content Methods, along with any additional Extended Data display items and Source Data, are available in the online version of the paper; references unique to these sections appear only in the online paper.

Received 29 March; accepted 13 August 2014.

- Whipple, K. X. The influence of climate on the tectonic evolution of mountain belts. *Nature Geosci.* **2**, 97–104 (2009).
- Whipple, K. X., DiBiase, R. A. & Crosby, B. T. in *Treatise on Geomorphology* (eds Shroder, J. & Wohl, E.) Vol. 9 *Fluvial Geomorphology* 550–573 (Academic Press, 2013).
- Sklar, L. S. & Dietrich, W. E. A mechanistic model for river incision into bedrock by saltating bed load. *Wat. Resour. Res.* **40**, W06301 (2004).
- Lamb, M. P., Dietrich, W. E. & Sklar, L. S. A model for fluvial bedrock incision by impacting suspended and bed load sediment. *J. Geophys. Res.* **113**, F03025 (2008).
- Chatanantavet, P. & Parker, G. Physically based modeling of bedrock incision by abrasion, plucking, and macroabrasion. *J. Geophys. Res.* **114**, F04018 (2009).
- Ferrier, K. L., Huppert, K. L. & Perron, J. T. Climatic control of bedrock incision. *Nature* **496**, 206–209 (2013).
- Finnegan, N. J., Schumer, R. & Finnegan, S. A signature of transience in bedrock river incision rates over timescales of 10^4 – 10^7 years. *Nature* **505**, 391–394 (2014).
- Willett, S. D. *et al.* Dynamic reorganization of river basins. *Science* **343**, <http://dx.doi.org/10.1126/science.1248765> (2014).
- Howard, A. D. & Kerby, G. Channel changes in badlands. *Geol. Soc. Am. Bull.* **94**, 739–752 (1983).
- Seidl, M. A. & Dietrich, W. E. The problem of channel erosion into bedrock. *Catena* (Suppl.) **23**, 101–124 (1992).
- Howard, A. D., Dietrich, W. E. & Seidl, M. A. Modeling fluvial erosion on regional and continental scales. *J. Geophys. Res.* **99**, 13971–13986 (1994).
- Seidl, M. A., Dietrich, W. E. & Kirchner, J. W. Longitudinal profile development into bedrock: an analysis of Hawaiian channels. *J. Geol.* **102**, 457–474 (1994).
- Stark, C. P. A self-regulating model of bedrock river channel geometry. *Geophys. Res. Lett.* **33**, L04402 (2006).
- Barbour, J. R. *et al.* Magnitude-frequency distributions of boundary shear stress along a rapidly eroding bedrock river. *Geophys. Res. Lett.* **36**, L04401 (2009).
- Turovskii, J. M., Lague, D. & Hovius, N. Response of bedrock channel width to tectonic forcing: insights from a numerical model, theoretical considerations, and comparison with field data. *J. Geophys. Res.* **114**, F03016 (2009).
- DiBiase, R. A. & Whipple, K. X. The influence of erosion thresholds and runoff variability on the relationships among topography, climate, and erosion rate. *J. Geophys. Res.* **116**, F04036 (2011).
- Tucker, G. E. & Hancock, G. R. Modelling landscape evolution. *Earth Surf. Process. Landf.* **35**, 28–50 (2010).
- Howard, A. D. A detachment-limited model of drainage basin evolution. *Wat. Resour. Res.* **30**, 2261–2285 (1994).
- Nelson, P. A. & Seminara, G. Modeling the evolution of bedrock channel shape with erosion from saltating bed load. *Geophys. Res. Lett.* **38**, L17406 (2011).

20. Wobus, C. W., Tucker, G. E. & Anderson, R. S. Self-formed bedrock channels. *Geophys. Res. Lett.* **33**, L18408 (2006).
21. Leopold, L. B., Wolman, M. G. & Miller, J. P. *Fluvial Processes in Geomorphology* (Freeman, 1964).
22. Venditti, J. G. *et al.* (eds) in *Coherent Flow Structures at Earth's Surface* 1–16 (Wiley, 2013).
23. MacVicar, B. J. & Rennie, C. D. Flow and turbulence redistribution in a straight artificial pool. *Wat. Resour. Res.* **48**, W02503 (2012).
24. MacVicar, B. J., Obach, L. & Best, J. L. in *Coherent Flow Structures at Earth's Surface* (eds Venditti, J. G. *et al.*) 243–259 (Wiley, 2013).
25. Nezu, I. & Nakagawa, H. *Turbulence in Open-Channel Flows* 96–110 (A. A. Balkema, 1993).
26. Yang, S.-Q. Velocity distribution and wake-law in gradually decelerating flows. *J. Hydraul. Res.* **47**, 177–184 (2009).
27. Finnegan, N. J., Sklar, L. S. & Fuller, T. K. Interplay of sediment supply, river incision, and channel morphology revealed by the transient evolution of an experimental bedrock channel. *J. Geophys. Res.* **112**, F03S11 (2007).
28. Fuller, T. K. *Field, Experimental and Numerical Investigations into the Mechanisms and Drivers of Lateral Erosion in Bedrock Rivers*. PhD thesis, Univ. Minnesota (2013).

Supplementary Information is available in the online version of the paper.

Acknowledgements This study was supported by Natural Science and Engineering Research Council grants to M.C., J.G.V. and C.D.R. We thank D. Baerg and his crew at Fraser River Raft Expeditions for undertaking the logistics of the river traverse, R. DiBiase for reviewing an early draft of the manuscript, and M. Lin and C. Adderley for assistance with data processing.

Author Contributions M.C. planned and organized the field campaign and provided guidance through the analysis. J.G.V., C.D.R. and M.C. performed the survey and supervised data processing and analysis by J.B., R.W.B and M.L. J.G.V. analysed the data and wrote the manuscript with input from C.D.R. and M.C.

Author Information Reprints and permissions information is available at www.nature.com/reprints. The authors declare no competing financial interests. Readers are welcome to comment on the online version of the paper. Correspondence and requests for materials should be addressed to J.G.V. (jeremy_venditti@sfu.ca).

METHODS

Observations. The Fraser River drains 228,000 km² of southwestern British Columbia. It is a snowmelt-dominated system with high flows between May and July. We undertook a 524-km continuous centreline transect using a four-beam 1,200-kHz acoustic Doppler current profiler (ADCP; RD Instruments) between 15 and 22 September 2009, on the falling limb of the annual hydrograph. Discharge varied between 861 m³ s⁻¹ (at Marguerite) and 1,760 m³ s⁻¹ (at Hope); nearly all the difference being due to tributary inflows. We extracted velocity profiles in 39 of the 42 bedrock canyons between Quesnel and Chilliwack (Extended Data Fig. 1). We present vertical velocity profiles from the centreline transect in Iron Canyon, where distance between profiles was typically less than 5 m. In Black Canyon (Extended Data Fig. 2a) we measured three-dimensional velocity profiles in a zigzag pattern, which produces data ideal for interpolation by kriging²⁹. The distance along the right or left banks that separated the location at which the boat was turned to cross the river again was typically less than 5 m. Each velocity profile was measured using the broadband 'Water Mode 1' ADCP instrument setting, with a vertical resolution of 0.25 m.

Data processing. Raw velocity profile data were processed with software developed by Rennie and collaborators^{29,30}. Only four-beam velocity solutions were used, reducing the potential for calculation of velocity using a beam that impinged upon the canyon walls. The redundant fourth ADCP beam provides an additional velocity component, from which a horizontal 'error velocity' is calculated. The error velocity accounts for both acoustic noise and heterogeneity of flow between the four acoustic beams.

In Iron Canyon we present the primary downstream velocity because it represents the local streamwise velocity with the cross-stream component of the integrated velocity profile minimized³¹, which is ideal for calculation of the shear stress from individual profiles. The alongstream, centreline transect profiles of primary downstream velocity (Fig. 1) were processed with an 11-point moving average to reduce variability caused by local turbulence and measurement error. The plunging flow structure is visible without the running average.

In Black Canyon (Fig. 2 and Supplementary Videos 1 and 2), no moving average was applied to the data. Lateral separation between velocity profiles was about 1 m, producing 3,470 profiles through the entrance to the canyon (Extended Data Fig. 2b). The single-ping, single-bin mean absolute error velocity in the Black Canyon spatial survey was 0.44 m s⁻¹, which was less than the mean and standard deviation of the horizontal velocity magnitude of 2.02 m s⁻¹ and 0.81 m s⁻¹, respectively. Relative errors (error velocity magnitude normalized by horizontal velocity magnitude) did not exceed 17%, and were less than 5% on average in Black Canyon. Relative errors did not show any spatial trend other than increased values near locations of variable bathymetry.

In Black Canyon we calculated the position at which each of the ADCP's four acoustic beams sensed the canyon boundary and corrected for the beam angle, which produced 14,709 bathymetry measurements (Extended Data Fig. 2c) to produce canyon bed topography (Extended Data Fig. 3). The velocity data were interpolated by kriging onto a regular 2-m horizontal and 0.25-m vertical three-dimensional grid (see Extended Data Fig. 4 for an example) that was then sliced to produce cross-sections like those in Fig. 2 and Supplementary Videos 1 and 2. The spatial interpolation reduced variability due to turbulence and measurement error³⁰, and allowed for identification of the flow structure. We also interpolated the data at higher densities (1 m and 0.5 m) and found it had little effect on the flow structure we observe.

Animations of the cross-stream slices of the horizontal velocity magnitude (Supplementary Video 1) and vertical velocity (Supplementary Video 2) grids in Black Canyon are available in the Supplementary Information. Supplementary Video 1 shows that after the initial channel constriction, a velocity inversion forms and persists through the entire canyon. The velocity inversion becomes more pronounced when it passes through the channel constriction halfway along the canyon, forming a high-velocity core near the bed. Supplementary Video 2 shows downward-directed

velocity through most of the canyon. Immediately downstream of the channel constriction, halfway along the canyon, we observe downward-directed flow in the channel centre and vertical flow up the channel walls.

Calculation of shear stresses. Reach-averaged shear stresses are derived from the one-dimensional momentum balance for steady uniform flow, calculated as:

$$\tau = \rho g S h \quad (1)$$

where ρ is water density, g is gravitational acceleration, S is the water surface slope in the canyon, and h is the mean flow depth in the canyon. This form of the momentum equation assumes that the flow is not changing through time or space. The latter assumption is clearly violated because the bed and water surface must be parallel for uniform flow (Fig. 1), which is why we use reach-averaged mean depth and water surface slope in the canyon. The reach-averaged shear stress is the total stress applied to the boundary. There is no wall-correction method for narrow channels where the roughness is the same on the walls and the bed. However, DiBiase and Whipple¹⁶ explored the ratio of shear stresses applied to the bed and the walls using an isoray model^{19,32}. They found that the bed shear stress is about half of the total shear stress in canyons with a width to depth ratio of approximately 2.5. They also found that using the hydraulic radius to account for the shear stresses on the walls, as is often done in lowland rivers, overpredicts the bed shear stress in narrow canyons (R. DiBiase, personal communication, 17 February 2014). So the shear stress calculated from equation (1) is corrected by dividing it by 2.

Shear stresses are also derived from the velocity gradient m calculated using a least-squares regression between the $\ln(z)$ and u , where u is the velocity at elevation z above the bed. The shear velocity is calculated as:

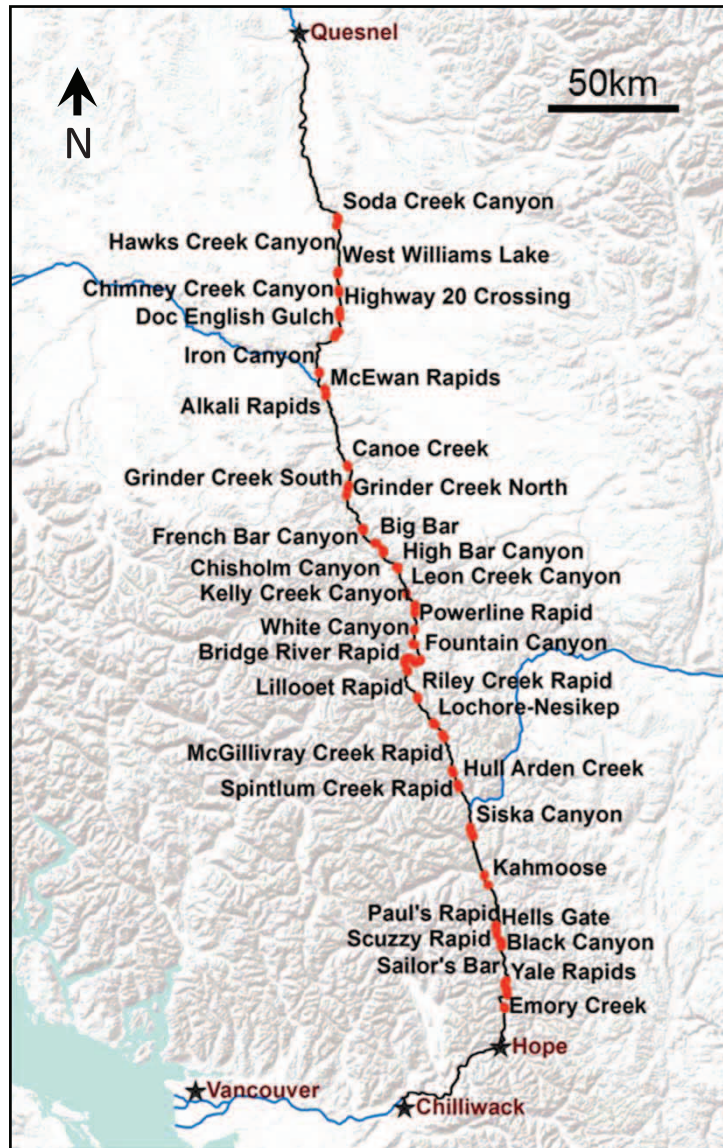
$$u_* = m \kappa \quad (2)$$

where κ is the von Karman constant equal to 0.41 and the shear stress is calculated as:

$$\tau = \rho u_*^2 \quad (3)$$

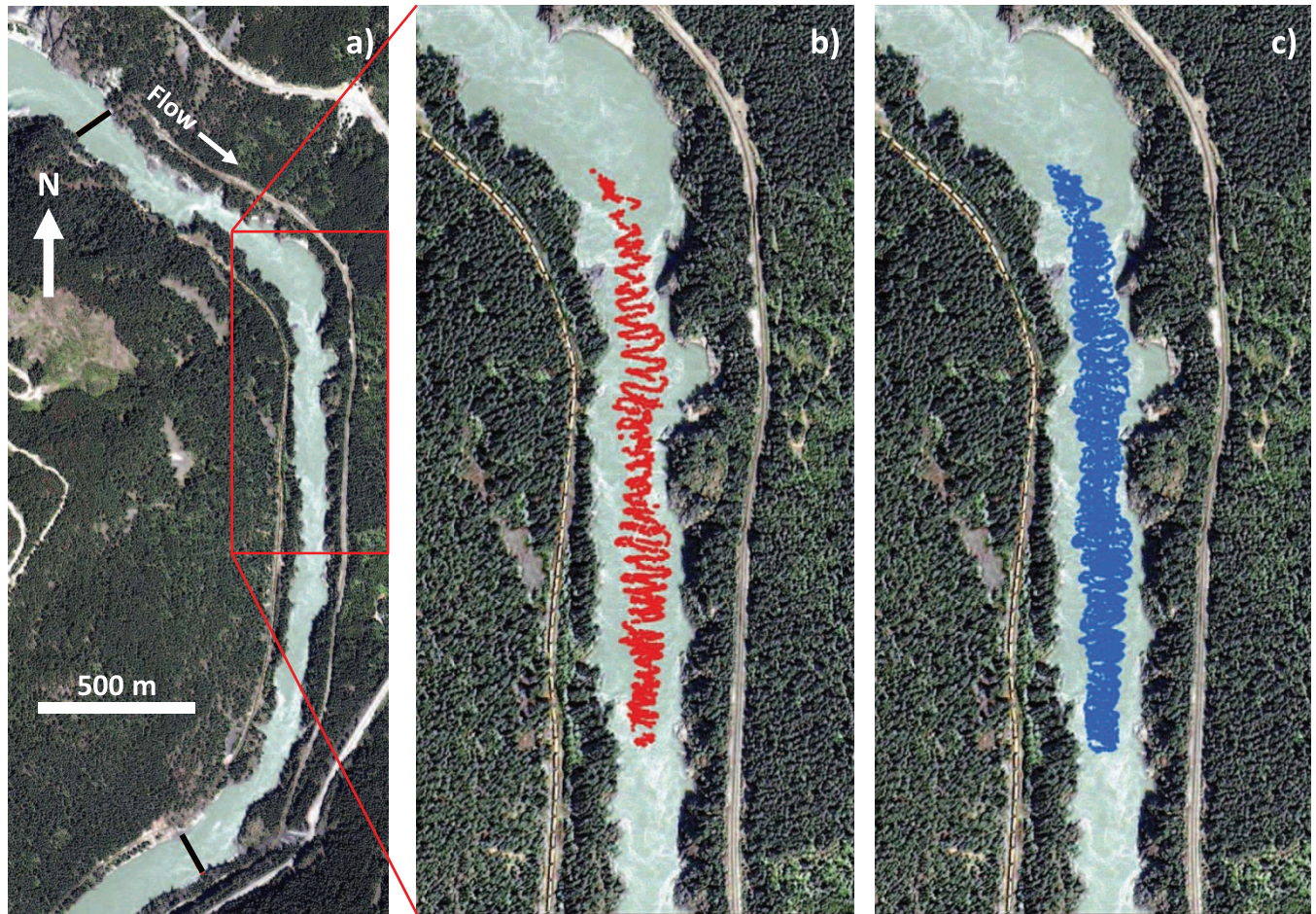
We do this for velocity profiles through the whole water column, as is usually done in rivers because they are depth-limited, and for the lower linear portion of the velocity inversion. Profile groups A and F have no inflection point (Fig. 1b), so we use the whole profile in both calculations of shear stress. Profile groups B, C and E (two of three profiles) have a linear portion of the profile that extends from the inflection point (velocity maximum) to the bed (Fig. 1b). Profile groups D and E (one of three profiles) have linear profiles near the bed only, well below the height of the inflection point (Fig. 1b). The velocity gradient approximation of the shear stress also assumes local steady, uniform flow, but has been shown to accurately predict shear stresses in non-uniform flow, as long as the log-linear portion of the velocity profile is near the bed³³, which is why we use the lower portion of the velocity inversion. All regressions exclude data in the lower 6% of the flow where acoustic sidelobe interference affects velocity accuracy. Each data point we present in Fig. 1c is an average of three or four shear stress estimates from the velocity profiles in Fig. 1b at each location shown in Fig. 1a.

29. Rennie, C. D. & Church, M. Mapping spatial distributions and uncertainty of water and sediment flux in a large gravel bed river reach using an acoustic Doppler current profiler. *J. Geophys. Res.* **115**, F03035 (2010).
30. Jamieson, E. C. et al. 3-D flow and scour near a submerged wing dike: ADCP measurements on the Missouri River. *Wat. Resour. Res.* **47**, W07544 (2011).
31. Bathurst, J. C., Thorne, C. R. & Hey, R. D. Direct measurements of secondary currents in river bends. *Nature* **269**, 504–506 (1977).
32. Kean, J. W. & Smith, J. D. in *Riparian Vegetation and Fluvial Geomorphology* (eds Bennett S. J. & Simon, A.) 237–252 (AGU, 2004).
33. Kironoto, B. A. & Graf, W. H. Turbulence characteristics in rough non-uniform open-channel flow. *Proc. ICE* **112**, 336–348 (1995).



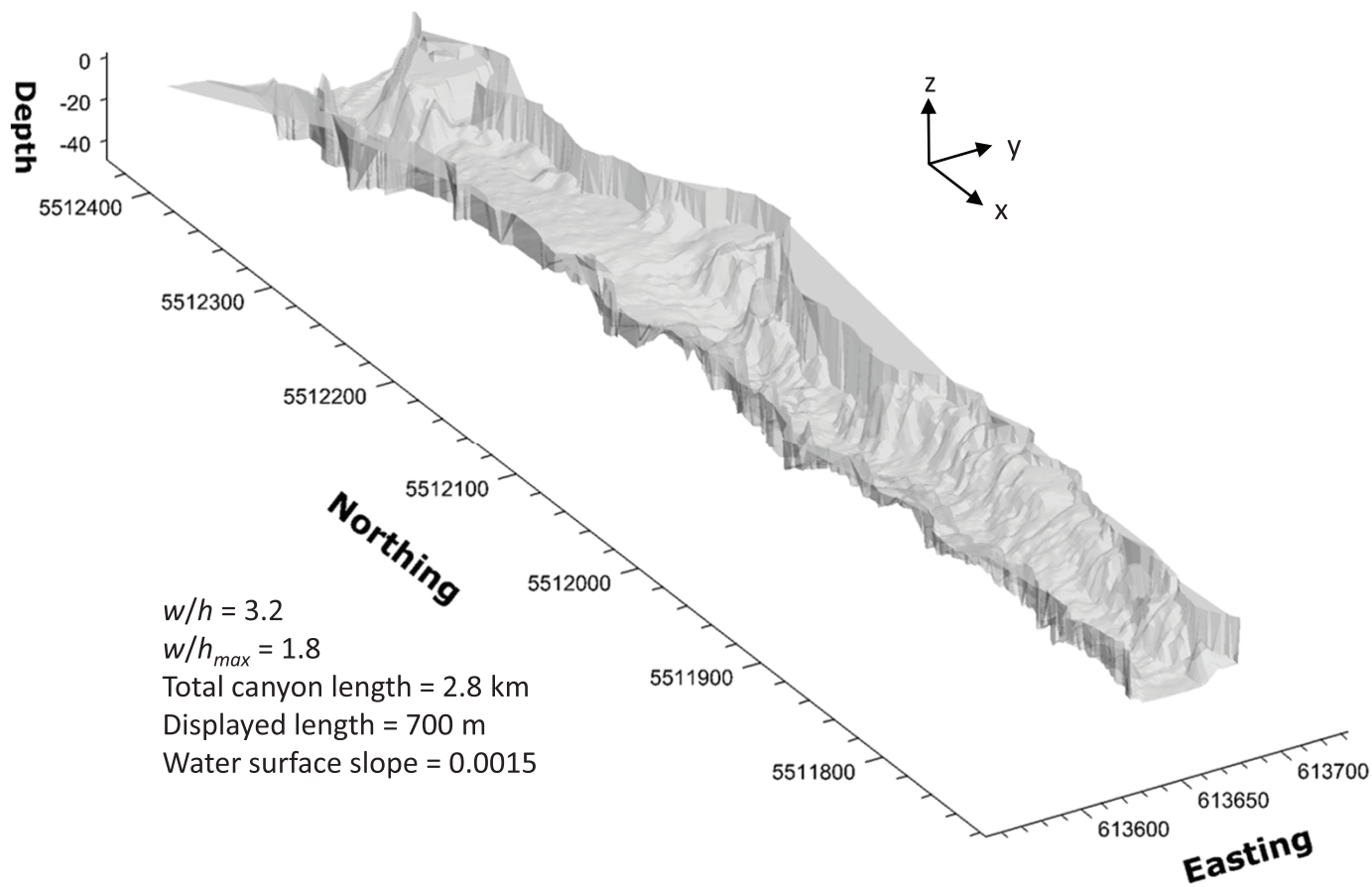
Extended Data Figure 1 | Bedrock canyons of the Fraser River, British Columbia. From Quesnel to Yale, the river crosses the Interior Plateau where the surficial rock is dominantly volcanic, with sedimentary rock along the river.

From Lillooet Rapid to Chilliwack, the river flows along a fault between the Coast Mountains to the west and the Cascade Mountains to the east.



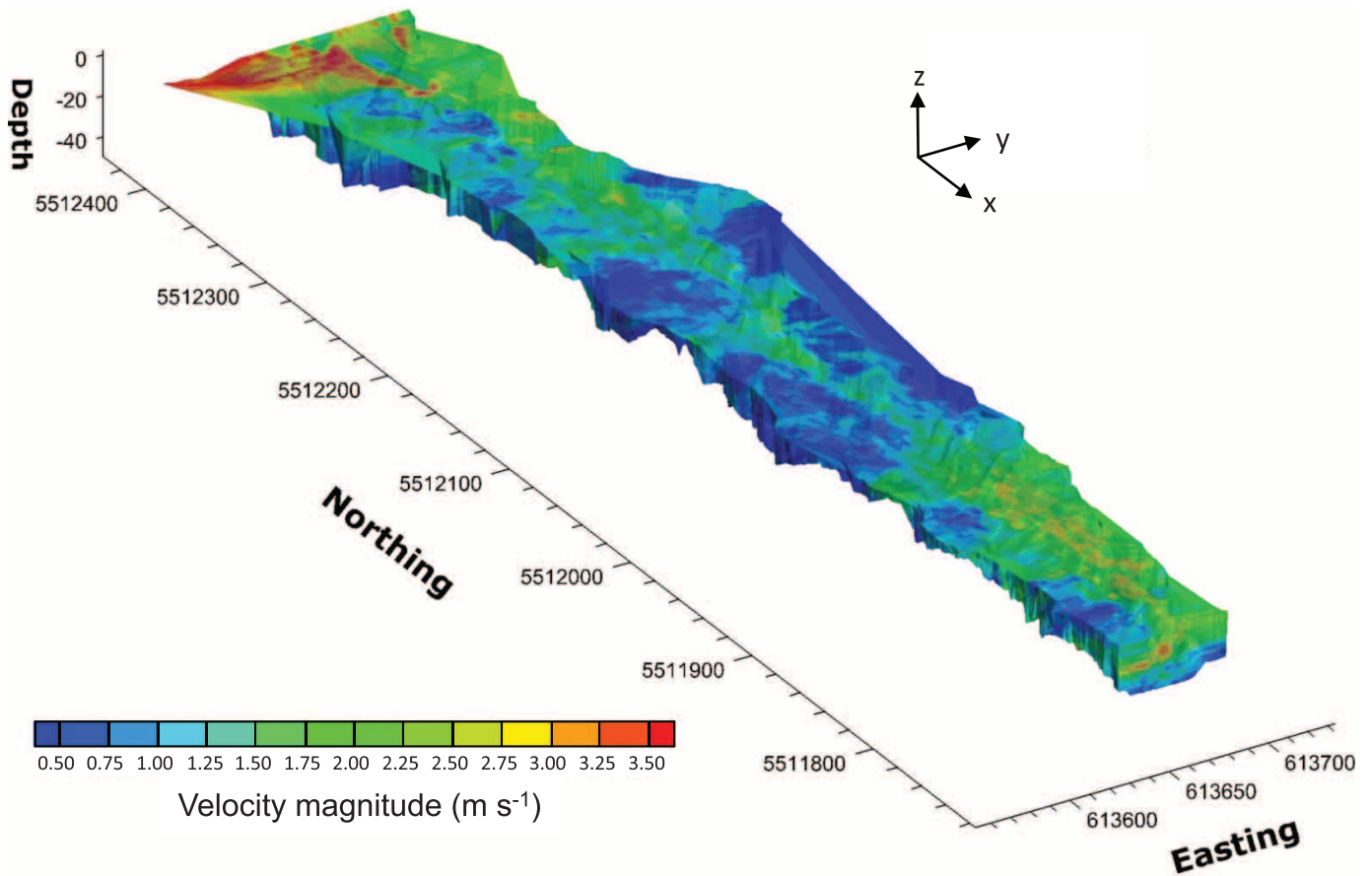
Extended Data Figure 2 | ADCP measurement survey through the entrance to Black Canyon. a, Satellite image of Black Canyon with black lines across the channel marking the entrance and exit of the canyon. b, Velocity profile measurement locations (red dots) obtained using the 1,200-kHz ADCP. The

surveyed length was 700 m. c, Bed topography measurement locations (blue dots) from the ADCP. The image is from the Ikonos satellite on 11 July 2007, processed by GeoEye/DigitalGlobe and accessed via ESRI ArcGIS software (<http://www.esri.com/>).



Extended Data Figure 3 | Interpolated bed topography at the entrance to Black Canyon. Interpolated using kriging onto a regular 2 m grid. Canyon walls were assumed to be vertical where there are no other data available. The

channel margins are defined by the water level in aerial photos, where discharge is approximately $6,440 \text{ m}^3 \text{ s}^{-1}$ at Hope.



Extended Data Figure 4 | Example of an interpolated velocity magnitude grid in Black Canyon. Velocity magnitude is defined as $(U_n^2 + U_e^2 + U_w^2)^{0.5}$, where U_n is the Northing, U_e is the Easting and U_w is the vertical velocity. The interpolation is done in Tecplot (<http://www.tecplot.com/>) software using

kriging on a three-dimensional grid generated using the prism grid function with a vertical resolution of 0.25 m, and a horizontal resolution of 2 m. Interpolated velocities are shown with a 30% transparency so that all data in the three-dimensional grid can be seen.